THE ASTROPHYSICAL JOURNAL, 565:571–586, 2002 January 20

BORON ABUNDANCES IN B-TYPE STARS: A TEST OF ROTATIONAL DEPLETION DURING MAIN-SEQUENCE EVOLUTION[1]

K. A. VENN[2] AND A. M. BROOKS
Macalester College, Saint Paul, MN 55105

DAVID L. LAMBERT
University of Texas at Austin, Austin, TX 78712

M. LEMKE
Dr. Karl Remeis-Sternwarte Bamberg, Sternwartstrasse 7, Bamberg D-96049, Germany

N. LANGER
Department of Physics and Astronomy, University of Utrecht, P.O. Box 80000, Utrecht, TA 3508, Netherlands

D. J. LENNON
Isaac Newton Group of Telescopes, Apatado de Correos 321, Santa Cruz de La Palma, Canary Islands E-38780, Spain

AND

F. P. KEENAN
Department of Pure and Applied Physics, the Queen's University of Belfast, Belfast BT7 1NN, Northern Ireland
Received 2001 July 5; accepted 2001 September 18

ABSTRACT

Boron abundances have been derived for seven main-sequence B-type stars from *Hubble Space Telescope* STIS spectra around the B III λ2066 line. In two stars, boron appears to be undepleted with respect to the presumed initial abundance. In one star, boron is detectable but is clearly depleted. In the other four stars, boron is undetectable, implying depletions of 1–2 dex. Three of these four stars are nitrogen enriched, but the fourth shows no enrichment of nitrogen. Only rotationally induced mixing predicts that boron depletions are unaccompanied by nitrogen enrichments. The inferred rate of boron depletion from our observations is in good agreement with these predictions. Other boron-depleted nitrogen-normal stars are identified from the literature. In addition, several boron-depleted nitrogen-rich stars are identified, and while all fall on the boron-nitrogen trend predicted by rotationally induced mixing, a majority have nitrogen enrichments that are not *uniquely* explained by rotation. The spectra have also been used to determine iron group (Cr, Mn, Fe, and Ni) abundances. The seven B-type stars have near-solar iron group abundances, as expected for young stars in the solar neighborhood. We have also analyzed the halo B-type star PG 0832+676. We find [Fe/H] = -0.88 ± 0.10, and the absence of the B III line gives the upper limit [B/H] < -2.5. These and other published abundances are used to infer the star's evolutionary status as a post–asymptotic giant branch star.

Subject headings: stars: abundances — stars: evolution — stars: rotation

1. INTRODUCTION

The light trace elements lithium, beryllium, and boron (LiBeB) are at the center of astrophysical puzzles involving sites as diverse as the primordial fireball, interstellar (IS) or even intergalactic space, and stellar surfaces and interiors. This paper is concerned primarily with boron's role in testing models of stellar interiors and evolution. This role arises because boron nuclei are destroyed by warm protons, and thus even quite shallow mixing of the atmosphere with the interior reduces the surface abundance by bringing boron-depleted material to the surface. Lithium and beryllium are similarly affected. Thus, a determination that the surface abundance of a light element is less than the star's initial abundance is an observational constraint for testing models of stellar interiors.

Lithium has served to test models of cool stars at essentially all phases of evolution, from the pre–main-sequence through to the post–asymptotic giant branch (post-AGB) stage, with the atomic resonance doublet conveniently placed at 6707 Å. Beryllium has seen similar but limited use through the Be II λ3130 resonance doublet. Boron has seen little use in testing mixing and other processes (e.g., mass loss) owing to the location of its resonance lines of B I, B II, and B III in the ultraviolet. This is unfortunate because boron alone is observable in hot stars.

In the case of hot stars, boron abundances have been determined using the B II λ1362 resonance line by Boesgaard & Heacox (1978) using *Copernicus* data, by Venn, Lambert, & Lemke (1996) using *IUE* data, and by Cunha et al. (1997) from the GHRS on the *Hubble Space Telescope* (*HST*). However, in stars of mid-B and earlier spectral types, boron is predominantly present as B III, not B II. Proffitt et al. (1999) were the first to use the B III λ2066 line to determine boron abundances and $^{11}B/^{10}B$ isotopic ratios in three B-type stars from very high signal-to-noise ratio (S/N) *HST* GHRS spectra. Subsequently, Proffitt & Quigley (2001, hereafter PQ01) mined the *IUE* archive for high-resolution spectra of B-type stars and reported boron abundances or upper limits for 44 early B-type stars.

A principal goal of most of these studies of hot stars was to establish the present-day boron abundance in order to

[1] Based on observations made with the NASA/ESA *Hubble Space Telescope*, obtained at the Space Telescope Science Institute, which is operated by the Association of Universities for Research in Astronomy, Inc., under NASA contract NAS 5-26555. These observations are associated with proposal GO 07400.

[2] Department of Astronomy, University of Minnesota, 116 Church Street, Minneapolis, MN 55455.

improve our understanding of the Galactic chemical evolution of boron. In this paper our primary goal is different: we are searching for boron-depleted stars to understand how their depletion arose. Only PQ01 have shared this goal. Herein we shall describe a test of rotationally induced mixing in rapidly rotating massive stars. Shallow mixing results in the destruction of boron (lithium and beryllium also) by proton capture. Deeper mixing also penetrates regions where H burning via the CN cycle has converted carbon into nitrogen. From any deep mixing, one may thus anticipate a drop in the surface abundance of boron, followed by a continued decline in boron accompanied by a nitrogen enrichment and carbon depletion as the star ages on the main sequence.

New stellar evolution models that include the effects of rotationally induced mixing (Heger & Langer 2000, hereafter HL00; Maeder & Meynet 2000) predict that boron is depleted during main-sequence evolution. Fliegner, Langer, & Venn (1996) first predicted a boron-nitrogen relationship in rotating stars and suggested it as an observational test of rotational mixing in hot stars. This test is unique since boron and nitrogen abundance variations, and the boron-nitrogen relationship predicted, cannot be explained by simple initial abundance variations, nor binary evolution with mass transfer (e.g., Wellstein, Langer, & Braun 2001; Wellstein 2000; discussed further below). Extraordinary mass-loss rates for B-type main-sequence stars are demanded if surface boron depletions are to occur through exposure of boron-depleted layers. The lifetime of ^{11}B and ^{10}B against proton capture equals the main-sequence lifetime of about 10^7 yr at an internal layer with a temperature of about 7×10^6 K. Above this layer resides about $\sim 1\ M_\odot$ of material (see Fig. 1 in Fliegner et al. 1996; Figs. 2, 3, and 4 in HL00), and therefore a mass-loss rate of $\sim 10^{-7}\ M_\odot\ \mathrm{yr}^{-1}$ is required if surface boron depletions are to occur. Such a rate is typical of B-type supergiants but at least an order of magnitude larger than derived for main-sequence OB stars (Cassinelli et al. 1994). The new rotating stellar evolution models also address other long-standing problems (beyond abundance anomalies), such as the origins of B[e] and WNL/Ofpe (slash) stars, the distribution of blue-to-red supergiants in the H-R diagram, and the unseen post–main-sequence gap predicted in all standard stellar evolution scenarios (see Langer & Heger 1999).

In this paper we present boron abundances from the B III λ2066 line from new *HST* STIS spectra of seven Galactic main-sequence B-type stars. These stars were selected from a variety of OB associations and have been well studied in the optical so that atmospheric parameters and surface nitrogen and carbon abundances are available in the literature. We have also used the spectra to determine their iron group abundances, which are difficult to determine accurately from optical studies of B-type stars, as a result of a lack of Fe III lines and uncertainties in non-LTE (NLTE) effects on available lines.

Our observing program included an eighth star, PG 0832+676, a B-type star in the halo, whose evolutionary status has been debated for a number of years. Brown et al. (1989) deduced that the star was a normal Population I B1 V object at a Galactocentric distance of $R_G \sim 37$ kpc and $z \sim 18$ kpc from the Galactic plane. Hambly et al. (1996) reanalyzed this star and found that α-elements (Mg, Al, Si, S) were underabundant by about 0.4 dex relative to HR 1886, a local B-type star. These authors argued that the star was not an H-burning star but rather was either a blue horizontal branch or a post-AGB star. Our spectra provide not only an estimate of the boron abundance but also new iron group abundances (Hambly et al. 1996 detected one Fe III line, which suggested [Fe/H] ~ -0.5 from a differential analysis). We will use these abundances to further establish the star's evolutionary status. In addition, as Hambly et al. (1996) noted, PG 0832+676 is extremely sharp lined, and as such its ultraviolet spectrum could provide a superb template for line identifications and wavelength calibrations.

2. TARGET SELECTION AND OBSERVATIONS

Eight B-type stars were selected for *HST* STIS spectroscopy near the B III λ2066 line (see Table 1). Five of these targets are bright stars in OB associations. Our goal was to select well-studied stars with a range of carbon and nitrogen abundances, and located in OB associations of different ages, in order to search for trends in the boron abundances with these parameters. A sixth target is the bright star HD 34078, a runaway OB star from Ori OB1. These six bright objects are also known variable stars (typically, β Cep variables; this seems to have no influence on the surface abundances, discussed below), and two are in known binary systems (see Table 2). Two fainter targets are also included: BD +56°576 in Per OB1 and PG 0832+676 in the Galactic halo. All of our targets have well-determined atmospheric parameters (see Table 3).

Careful planning was necessary to avoid the MAMA–near-UV brightness limits in observing the six bright targets. Even the most narrow slit, with the high-resolution E230H grating ($R = 114{,}000$), was rarely permitted for our observations. This combination worked only for HD 34078 at $V = 6.0$. For the other brighter objects, it was necessary to use either the lower resolution E230M grating ($R = 30{,}000$) or E230H with a neutral density filter, 0.2×0.05ND (ND = 2), to obtain our spectra in the minimum number of orbits (see Table 1). The E230M grating is sufficient to resolve the B III line in all of our targets; the instrumental broadening for this grating is 9 km s^{-1} (± 1 km s^{-1} depending on the slit choice), whereas the targets have measured rotational velocities ranging from $1 \leq v \sin i \leq 39$ km s^{-1}. For the faint star, PG 0832+676, the E230M grating and 0.2×0.2 slit combination produced a good-quality spectrum for the abundance analysis, but we were not able to take full advantage of the sharp-lined nature of PG 0832+676 as a UV spectral template.

Multiple exposures were taken at slightly varying central wavelengths to maximize the S/N at the B III λ2066 line for most objects. The exposure times and central wavelengths are listed in Table 1. Spectra were reduced using the STIS pipeline. Each echelle observation included between 34 and 52 orders. We selected the order(s) that included the B III line in each exposure and combined these for maximum S/N near 2066 Å. The spectra were smoothed (3 pixel boxcar smoothing), rectified using a low-order Legendre polynomial, and offset from vacuum wavelengths (observed) to air wavelengths (line list, discussed below). Sample spectra are shown in Figures 1, 2, and 3. The resultant peak S/N values near 2066 Å are listed in Table 1. The final spectra used for iron group and boron abundance determinations in this paper range from 2045 to 2078 Å, with a dispersion ranging from ~ 4 (E230H) to ~ 16 km s^{-1} (E230M).

Four of the stars in this study are known β Cep variable

TABLE 1

HST STIS Observing Information for Galactic B stars

Star	V	Grat/Slit	Exposure (s)	Date	Total S/N
BD +56°576	9.38	E230M	1680 at λ_c2124	1999 Feb 11	100
		0.2 × 0.2	1280 at λ_c1978		
			1509 at λ_c2269		
HD 16582.....	4.07	E230H	1634 at λ_c2113	1999 Jan 23	90
		0.2 × 0.05ND	1140 at λ_c2063		
			1140 at λ_c2063		
			1368 at λ_c2013		
			1328 at λ_c2013		
HD 34078.....	6.00	E230H	432 at λ_c2063	2000 Mar 15	50
		0.1 × 0.03	432 at λ_c2013		
HD 36591.....	5.34	E230M	432 at λ_c2124	1999 Feb 09	100
		0.2 × 0.05ND	432 at λ_c2124		
			432 at λ_c2124		
			432 at λ_c1978		
			432 at λ_c1978		
			432 at λ_c2269		
			432 at λ_c2269		
HD 50707.....	4.83	E230M	216 at λ_c2124	1998 Nov 06	75
		0.2 × 0.05ND	216 at λ_c1978		
			216 at λ_c2269		
HD 205021	3.23	E230H	900 at λ_c2063	1999 Feb 19	100
		0.2 × 0.05ND	900 at λ_c2063		
			684 at λ_c2013		
			684 at λ_c2113		
			684 at λ_c1963		
HD 216916	5.59	E230M	1260 at λ_c2124	1998 Dec 16	130
		0.2 × 0.05ND	262 at λ_c2124		
			338 at λ_c2124		
			888 at λ_c1978		
			972 at λ_c2269		
PG 0832+676.....	14.15	E230M	3360 at λ_c2124	1998 Dec 08	100
		0.2 × 0.2	3360 at λ_c2124	CVZ	
			3360 at λ_c2124		
			3300 at λ_c2124		

stars (see Table 2). In fact, HD 205021 *is* β Cep. These stars exhibit variability in their radial velocities as well as their luminosities. For instance, HD 205021 displays a peak-to-trough amplitude of $\sim$40 km s^{-1} over a period of 0.19 days (Hadrava & Harmanec 1996). This period and amplitude are typical of the β Cep variables in our target list and are long enough to display radial velocity variations over the full range of our observations. However, the observations were divided into very short exposures to avoid the MAMA brightness limits. Thus, there is little significant broadening due to the radial velocity variations per exposure (typically about 4 km s^{-1}, although the longest exposure for HD 16582 may be broadened by as much as 9 km s^{-1}). As an additional test, we examined the FWHM of our individual

TABLE 2

Variability and Binary Information from the Literature

Star	Name	Variable	Binary	Cluster	Cluster Age (Myr)	References
BD +56°576	...	...	Eclipse	χ Per	11.5	1, 2, 3
HD 16582.....	δ Cet	β Cep	...	Cas-Tau	$\sim$50	4, 5, 6
HD 34078.....	AE Aur	Variable	Visual?	Ori OBI	...	7 (runaway)
HD 36591.....	...	Variable	Visual	Ori OBIb	1.7 $\pm$1.1	8, 9, 10, 11
HD 50707.....	15 CMa	β Cep	...	Coll 121	$\sim$5	4, 6
HD 205021	β Cep	β Cep	Spect	Cep OB1?	2 $\pm$1	12, 13, 14
HD 216916	16 Lac	β Cep	Eclipse	Lac OB1	12–16	6, 13, 15, 16, 17
PG 0832+676.....	...	...	...	Halo	...	...

References.—(1) Krzesiński & Pigulski 1997. (2) Oosterhoff 1937. (3) Tapia, Roth, & Navarro 1984. (4) Heynderickx, Waelkens, & Smeyers 1994. (5) Crawford 1963. (6) de Zeeuw et al. 1999. (7) Gies 1987. (8) Olsen 1977. (9) Brown & Verschueren 1997. (10) Warren & Hesser 1978. (11) Brown, de Geus, & de Zeeuw 1994. (12) Telting, Aerts, & Mathias 1997. (13) Fitch 1969. (14) Massey, Johnson, & Degioia-Eastwood 1995. (15) Pigulski & Jerzykiewicz 1988. (16) Jerzykiewicz & Pigulski 1999. (17) Blaauw 1991.

TABLE 3

ATMOSPHERIC PARAMETERS FROM THE LITERATURE

Star	Spectral Type	$T_{\rm eff}$ (K)	log g	$v \sin i$ (km s^{-1})	ξ (NLTE) (km s^{-1})	References
BD +56°576	B2 III	22500	3.40	<50[a]	9	1
	B2 III	21500	3.6	...	12	2
HD 16582.....	B2 IV	23750	4.08	15	3.8 ±5.1	3
HD 34078.....	O9.5 V	31420	4.07	27	8.0 ±0.6	3
HD 36591.....	B1 IV	27380	4.15	11	4.4 ±3.7	3
	B1 V	26330	4.21	...	9	4
HD 50707.....	B1 IV	27710	4.04	39	4.2 ±4.6	3
HD 205021	B1 IV	26740	4.16	28	3.3 ±3.7	3
HD 216916	B2 IV	24050	3.90	13	3.6 ±4.6	3
PG 0832+676.....	B1 V	23000	3.7	1	7 [b]	5

NOTE.—For BD +56°576 and HD 36591, the parameters from Vrancken et al. 2000 and GL92 were adopted, respectively.

[a] For BD +56°576, $v \sin i = 17$ km s^{-1} from our spectrum syntheses.

[b] ξ in PG 0832+676 from an LTE analysis.

REFERENCES.—(1) Vrancken et al. 2000. (2) Lennon, Brown, & Dufton 1988. (3) GL92. (4) CL94. (5) Hambly et al. 1996.

exposures and found insignificant differences in most cases. In the case of HD 216916, we were surprised to find no significant differences in the FWHM when comparing the 262, 880, and 1200 s exposures (although the amount of broadening due to radial velocity variations will also depend on the phase when the observation is taken). Finally, we shifted each spectrum into the stellar rest frame before co-addition to minimize smearing effects.

3. THE ABUNDANCE ANALYSES

Elemental abundances have been determined from LTE spectral syntheses and ATLAS9 model atmospheres (Kurucz 1979, 1988). Solar metallicity models were used throughout, with the exception of PG 0832+676 for which [Fe/H] = −1.0 models were adopted. LTE spectral syntheses were made using the program LINFOR.[3]

The stellar $T_{\rm eff}$, gravity, and projected rotational velocity ($v \sin i$) values were adopted from the literature (see Table 3). We note here that there is some uncertainty in the temperature scale for B-type main-sequence stars. This is discussed further in § 4. Other parameters were determined from the syntheses, i.e., macroturbulence, microturbulence (ξ), and radial velocity (see Table 4). Macroturbulence ($\xi_{\rm Ma}$) was initially set to the instrumental broadening values and then increased to best fit the spectral lines. In most cases, the macroturbulence is only 3–5 km s^{-1} larger than the smoothed instrumental profiles; however, HD 205021 and HD 16582 required macroturbulence values of 8 km s^{-1} larger. Observations for the latter two stars were made with E230H, which has a very sharp instrumental profile, thus much of the broadening in these two stars is likely due to

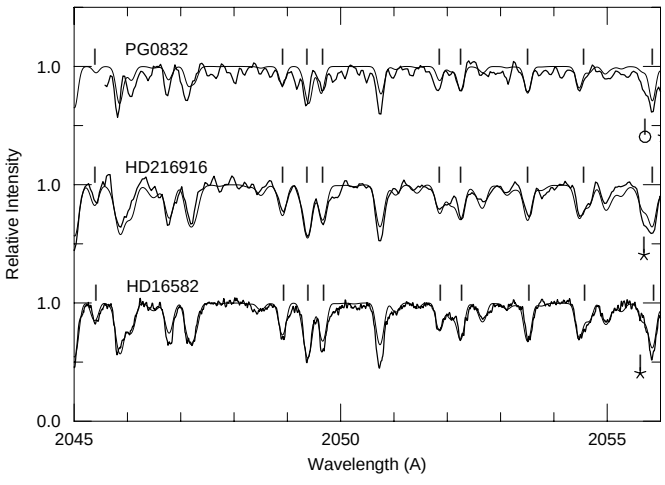

FIG. 1.—Co-added *HST* STIS spectra for three B-type stars (*thick line*) and their spectrum syntheses (*thin line*) in the range 2045–2056 Å. The observed spectra were smoothed for a 3 pixel resolution element, and the higher resolution from the E230H grating can be seen for HD 16582. The iron group metallicities in Table 6 were used for each synthesis. Features listed in Table 6 are identified. IS lines are marked below each spectrum; PG 0832+676 has two sets of IS lines.

[3] LINFOR was originally developed by H. Holweger, W. Steffen, and W. Steenbock at Kiel University. It has been upgraded and maintained by M. Lemke, with additional modifications by N. Przybilla.

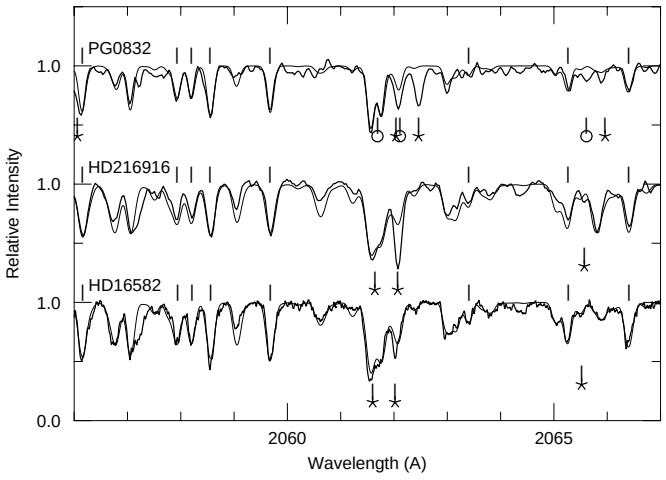

FIG. 2.—Same as Fig. 1, but for the range 2056–2067 Å

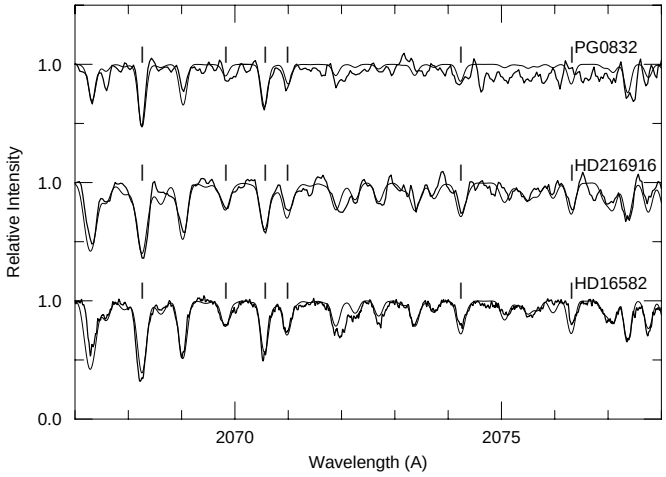

FIG. 3.—Same as Fig. 1, but for the range 2067–2078 Å

their β Cep radial velocity variations (discussed above). Another star, HD 34078, observed with E230H has a much lower macroturbulence and is not a known β Cep variable. A Gaussian line-spread function was adopted throughout our spectrum syntheses; while acceptable, we recognize that line-spread functions for the echelle gratings are available from STScI, but we neglected this specific instrumental broadening component in our syntheses.

Microturbulence was determined for each star using the Fe III lines, requiring that strong and weak lines yield the same iron abundance. Our ξ values are significantly lower than those in the literature from analyses of optical spectral lines (i.e., O II). This is not uncommon, as previously found by Venn et al. (1996) and Cunha et al. (1997), where ξ from UV analyses is significantly smaller than from optical analyses of the same star. This probably reflects differences in the structure of the upper atmosphere where the UV spectrum forms. Regardless, the value of ξ has little impact on the derived B III λ2065.8 line abundance (see below).

Only the BD +56°576 $v \sin i$ value was determined from syntheses since the upper limit in the literature was clearly too large. BD +56°576 and PG 0832+676 were observed with the same instrumental setup, thus the broadening parameters from the PG 0832+676 analysis were adopted for the BD +56°576 analysis. PG 0832+676 is a known sharp-lined object ($v \sin i = 1$ km s^{-1}), thus any remaining broadening required for BD +56°576 was attributed to its projected rotation rate.

3.1. *Line List*

Our spectral line list and atomic data originated from the Kurucz (1988; CD-ROM 18) line list, including all lines in the iron group, light-element, and heavy-element lists, up to barium, and through the fifth ionization state from titanium onward. We updated this line list by including the new wavelengths for eight Fe III lines reported by Proffitt et al. (1999) from Fourier transform spectrometer (FTS) laboratory measurements. We also updated the atomic data from Kurucz's semiempirical values for 64 Fe III lines from Ekberg (1993). Ekberg determined new wavelengths for the three lowest configurations of Fe III from laboratory measurements using a sliding spark discharge and spectrograph, with some energy levels computed assuming spin-orbit coupling, and transition probabilities calculated for all combinations.

Data for the B III $2s^2S$–$2p^2P$ resonance doublet with lines at 2065.8 and 2067.3 Å, and hyperfine and isotopic components, are taken from Proffitt et al. (1999). The line at 2065.8 Å, the stronger and less blended of the doublet, is our primary indicator of the boron abundance. This feature is blended with a weak Mn III line about 0.12 Å from the ^{11}B line and 0.08 Å from the ^{10}B line. In our spectra, the B III and the Mn III lines are not resolved. The Proffitt et al. (1999) high-S/N and high-resolution *HST* GHRS spectra of HD 35299 and HD 886 clearly show the contributions of the ^{10}B, ^{11}B, and Mn III lines separately. Their synthesis results for these two stars suggest that the Mn III wavelength should be offset by 6 mÅ redward of the Kurucz wavelength; also, they found that the abundance [Mn III] = −0.2 from that one feature, suggesting that the *gf*-value is 0.2 dex too large. We adopt the B III line list and transition probabilities given by Proffitt et al. (1999) and adjust the wavelength and oscillator strength of the blended Mn III line. (The weaker B III line at 2067.3 Å is blended with a strong Fe III line and weak Mn III line. The blending is of such severity that the λ2067.3 stellar line is not suitable for a boron abundance determination, although we note that the best boron fits to HD 216916, BD +56°576, and the upper limit for HD 36591 produce the best fit to the λ2067.3 B-Fe-Mn blend as well; see Figs. 4, 5, and 6.)

For all syntheses, we assume an isotopic ratio ^{11}B/^{10}B = 4.0, the solar system ratio (Shima 1963), consistent

TABLE 4

BORON AND IRON GROUP ABUNDANCES FROM STIS SPECTROSCOPY

Star	RV	ξ_{Ma}	ξ	[M/H]	log (B/H) LTE	log (B/H) NLTE	log (Mn III) λ2065.9
BD +56°576	1	20	4	−0.16 ± 0.17	2.43	2.25	5.24
HD 16582.....	12	12	2	−0.15 ± 0.15	1.27	1.16	5.31
HD 34078.....	56	7	3	−0.2 ± 0.2	≤2.0	≤2.2	5.1
HD 36591.....	31	18	2	0.02 ± 0.12	≤1.45	≤1.38	5.43
HD 50707.....	28	20	6	0.1 ± 0.1	≤1.5	≤1.5	5.4
HD 205021	−29	12	2	−0.16 ± 0.23	≤1.00	≤0.90	5.00
HD 216916	−18	19	1	0.16 ± 0.18	2.44	2.31	5.33
PG 0832+676.....	−68	20	2	−0.88 ± 0.10	≤0.75	≤0.60	4.65

NOTE.—Abundances have been determined from spectrum syntheses using the model atmosphere parameters listed here and in Table 3. Radial velocities (RV), ξ, and ξ_{Ma} (macroturbulence) values are determined from the iron group features. We estimate ΔRV and $\Delta\xi_{Ma} \sim 2$ km s^{-1} based on line profile shapes, and $\Delta\xi \leq 1$ km s^{-1}. The B III λ2065.8 and Mn III λ2065.9 abundances were allowed to vary independently for the best-fit syntheses, thus we report the Mn III λ2065.9 line abundance here.

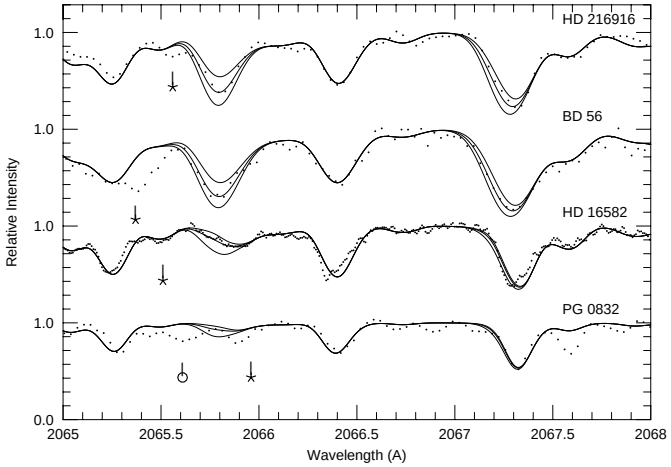

FIG. 4.—Boron syntheses for the three stars where the B III feature is detected and PG 0832+676. The best-fit syntheses are shown, as well as Δ log (B/H) = $\pm$0.4 for comparisons. IS lines are marked below each spectrum; PG 0832+676 has two sets of IS lines.

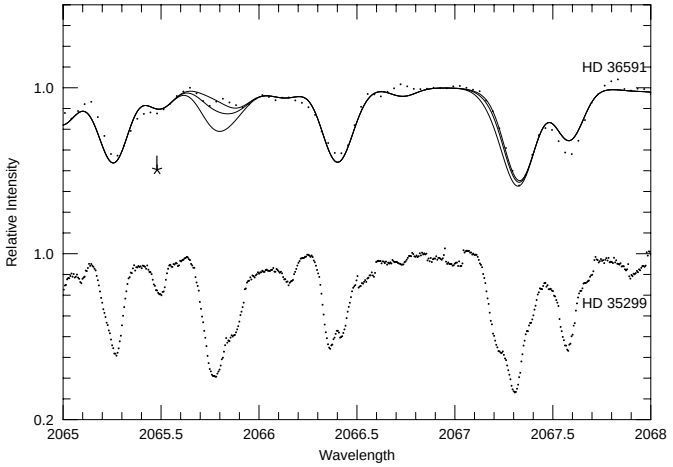

FIG. 6.—Boron syntheses for HD 36591; $12 + \log (B/H)_{LTE} = 1.05$, 1.45, and 1.85 are shown. Boron is clearly weak in HD 36591. For comparison, an *HST* GHRS spectrum for HD 35299 is shown. These two stars are both in the Orion OB1 association and have very similar atmospheric parameters, yet Proffitt et al. (1999) and Lemke et al. (2000) fit a normal LTE boron abundance to HD 35299 [$12 + \log (B/H) = 2.5$ and 2.7, respectively]. IS lines are marked for HD 36591.

with the estimates given by Proffitt et al. (1999) from their line profile analyses of two sharp-lined B-type stars. We also consider a smaller ratio in our boron uncertainty estimates (discussed below).

PQ01 first noted the importance of the IS lines in this wavelength range, particularly one Cr II IS line that comes close to the B III λ2065.8 feature depending on the stellar radial velocity. Since IS lines are quite sharp, we have identified their rest wavelengths from our spectrum of HD 205021. This star has a high S/N and rotation rate that make the broad stellar lines quite distinct from the sharp IS lines (see, e.g., Fig. 5). We have identified four IS lines as Cr II (2055.60, 2061.58, and 2065.50) and Zn II (2062.01) from Morton (1991). We note the locations of the IS lines in our spectrum figures (see Figs. 1–6), where the IS lines appear at different wavelengths because the (stellar) rest frame is used. The IS line near the B III feature is only a problem in PG 0832+676. PG 0832+676 has two sets of IS lines, one of which appears to be blended with the Mn III–B III λ2066 feature. This affects the accuracy of our upper limit for boron in PG 0832+676, but nevertheless, the boron feature is clearly absent (see Fig. 4). We also note in this figure that a Ti IV feature near 2067.6 Å in PG 0832+676 is not well fitted, but this is also seen in the spectrum of the hot star HD 34078, suggestive of atomic data uncertainties.

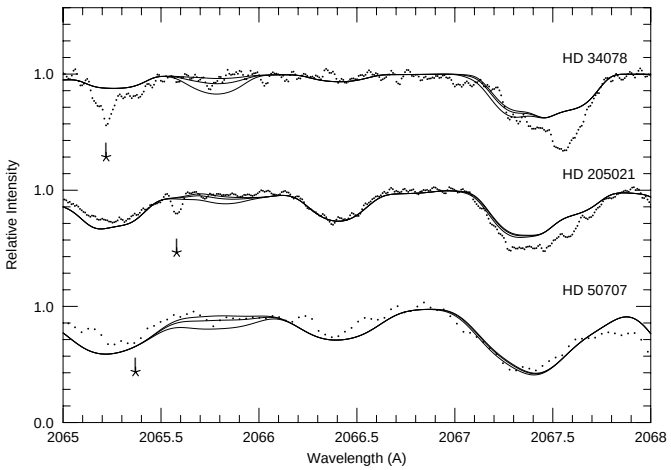

FIG. 5.—Boron syntheses for three stars where the B III feature is *not* detected (see Fig. 6 for HD 36591 synthesis). The best-fit syntheses are shown, as well as Δ log (B/H) = $\pm$0.4 for comparison. Clearly the boron abundance is more difficult to determine and less accurate in the broad-lined stars. IS lines are marked below each spectrum.

Our final line list includes 2275 features between 2045 and 2078 Å. All were included in the syntheses, but many are negligible contributors. A few final fine adjustments were made to the line list. We examined the preliminary syntheses of three of the sharp-lined stars in this sample, HD 216916, HD 36591, and PG 0832+676, and made slight wavelength shifts to improve the final spectrum syntheses. These fine adjustments are reported in Table 5. We made no fine adjustments to the oscillator strengths. It is worth noting that our final line list does a remarkably good job at fitting the UV spectrum in our stars. This is noteworthy because UV line lists are notoriously incomplete and/or uncertain in their atomic data. Examination of our spectrum figures shows very few missing lines and quite good fits, suggesting that the energy levels and transition probabilities are fairly accurate.

3.2. *Iron Group and Synthesis Parameters*

The iron group abundances were determined from examination of a number of clean features in the spectra. Spectrum syntheses of these individual features were performed and tabulated and the results averaged. This allowed us to minimize uncertainties due to poorly fitted lines, as well as lines which appear to have poor atomic data. In Table 6 we list the abundances relative to the meteoritic abundances from Grevesse & Sauval (1998), i.e., log (Fe) = 7.50 and log (Mn) = 5.53. The mean abundances in Table 6 were calculated by excluding line abundances that fall more than 2 σ (from the line-to-line scatter) from the mean.

We estimate an uncertainty of approximately $\pm$2 km s^{-1} in the macroturbulence, based on line profile fitting, but

TABLE 5

IRON GROUP WAVELENGTH OFFSETS

Element	λ(KUR)	λ(NEW)
Mn III.....	2048.949	2048.909
Mn III.....	2049.357	2049.314
Mn III.....	2049.682	2049.663
Mn III.....	2052.739	2052.673
Mn III.....	2063.337	2063.397
Mn III.....	2065.886	2065.892[a]
Fe III.....	2050.743	2050.738
Fe III.....	2052.271	2052.250
Fe III.....	2053.524	2053.508
Fe III.....	2054.492	2054.475
Fe III.....	2055.863	2055.848
Fe III.....	2056.152	2056.147
Fe III.....	2057.059	2057.052
Fe III.....	2058.209	2058.199
Fe III.....	2058.566	2058.558
Fe III.....	2059.692	2059.678
Fe III.....	2064.980	2065.030
Fe III.....	2068.896	2068.983
Fe III.....	2070.976	2070.976
Fe III.....	2076.322	2076.309
Ni III.....	2045.412	2045.387

NOTE.—Our line list originates from Kurucz 1988, with wavelengths for eight Fe III lines updated from Proffitt et al. 1999 and 64 others updated from Ekberg 1993 (wavelengths and *gf*-values). In this table we note additional adjustments to some line wavelengths based on our preliminary syntheses of sharp-lined stars in our sample. One line from Ekberg, λ2070.976, was moved back to the original Kurucz wavelength, but the new *gf*-value was retained.

[a] New wavelength from Proffitt et al. 1999, who also suggest log $gf = -0.241$. This feature is blended with the B III λ2065.8 line.

only ± 1 km s^{-1} in microturbulence based on line strengths. Effects of these uncertainties on the iron group abundances are quantified in Table 7 for a few representative stars. Uncertainties were found by fitting the iron group features listed in Table 6 individually and then averaging the changes. Continuum placement and the adopted ξ and macroturbulence parameters dominate the errors in the iron group abundances. NLTE effects are neglected throughout this iron group analysis. Iron group abundances are determined primarily from lines of the dominant species of the elements, e.g., Fe III, whose atomic statistical equilibrium rarely suffers from NLTE effects.

We find the mean iron group abundance of [Fe/H] $= -0.06 \pm 0.15$ from six to 23 features in seven main-sequence B-type stars. This is similar to the Cunha & Lambert (1994, hereafter CL94) results from one to eight optical lines of Fe III in 16 Orion OB1 B-type stars, [Fe/H] $= -0.05 \pm 0.10$, and also to the Gies & Lambert (1992, hereafter GL92) results from one to three optical lines of Fe II or Fe III in 31 Galactic B-type stars, [Fe/H] $= 0.22 \pm 0.20$. Six stars have *IUE* spectra that were examined by PQ01 for an overall scaling factor for heavy-element abundances. Although they note that the scaling factor per star should not be interpreted as a precise determination of the heavy-element abundance, we do note that their values are only about 0.2 dex lower than ours.

Finally, because of the uncertainties in the B-type main-sequence star temperature scale (discussed further in § 4), we note that a slight reduction in the GL92 temperatures (about 800 K, or 1 σ in the $T_{\rm eff}$ uncertainty) will reduce our mean iron group abundances by about 0.1 dex.

3.3. *Boron Abundances*

The LTE boron abundances listed in Table 4 are from spectrum syntheses, where we allowed the B III λ2065.8 and Mn III λ2065.9 line abundances to vary independently in order to achieve the best possible fit to the observation. Spectrum synthesis fits for all our program stars are shown in Figures 4, 5, and 6. We did not attempt to constrain the Mn III λ2065.9 line abundance, e.g., by setting the Mn abundance using other Mn III lines, because of uncertainties in the atomic data for other Mn III lines. We report the Mn III λ2065.9 line abundance determined from the best synthesis of the B III blended feature in each star in Table 4. It is in good agreement with the iron group abundances per star.

To compute the uncertainty in the boron abundances, Δ log (B/H), independent of uncertainties in Mn III λ2065.9, we found that it was necessary to fix the Mn III λ2065.9 line abundance a priori. Thus, we examined two methods (except for PG 0832+676, discussed below). Firstly, we simply set the value of Mn III from the best-fit synthesis (in Table 4) and then allowed only the B III line abundance to vary to calculate Δ log (B). Secondly, we applied the mean iron group corrections (in Table 7) to the Mn III line component and allowed boron to vary to find a new best fit for each uncertainty parameter. We found Δ log (B) to be very nearly identical from these two methods for all uncertainties investigated. The largest differences between the methods were ≤ 0.04 dex for $\Delta\xi_{\rm Ma}$ and $\Delta\xi$. In Table 8 we report the uncertainties from the latter method. Only for $\Delta V_{\rm rad}$ did we vary B III λ2065.8 and Mn III λ2065.9 together (both line abundance changes are reported in Table 8).

For PG 0832+676, we could not fit the B III–Mn III blend directly because of an IS line occurring near the location of the Mn III line. For this star, we computed the iron group abundances and applied that result for the Mn III λ2065.9 line abundance in order to determine a boron upper limit. We used this method since the Mn III λ2065.9 line abundance has been similar to the mean iron group abundance in all of the other stars, i.e., [Mn/Fe] $= -0.05$ to -0.35 (see Table 4 for Mn and Table 6 for Fe). If we applied a lower Mn III λ2065.9 line abundance (e.g., [Mn/Fe] $= -0.3$), then the change in the boron upper limit is small [e.g., Δ log (B/H) = 0.1].

In summary, Table 8 shows that the most significant uncertainties in the boron abundances tend to be the continuum placement (thus, S/N of the data also), and the radial velocity and assumed ^{11}B/^{10}B ratio (discussed further below) may be significant in some cases. In addition, the Mn III λ2065.9 atomic data could play an important role, but since the Mn abundance is not fixed for the boron syntheses, uncertainties in the Mn atomic data will be compensated in the fit. Thus, the boron abundances should be accurate to ± 0.1 dex. It is worth noting that lowering the temperature scale (discussed further in § 4) has a negligible effect on the boron abundances [Δ log (B/H) = 0.0 to -0.06].

Only for the hottest star, HD 34078, is the derived boron abundance significantly sensitive to uncertainties in the atmospheric parameters. In fact, examination of the predicted

TABLE 6

IRON GROUP ABUNDANCE RESULTS

λ (Å)	Element(s)	[M/H] BD 56	[M/H] 16582	[M/H] 34078	[M/H] 36591	[M/H] 50707	[M/H] 205021	[M/H] 216916	[M/H] PG 0832
2045.39	Ni III	...	−0.07	...	0.09	...	...	0.16	...
2048.91	Mn III	0.00	0.03	(0.5)	0.00	0.2[a]	−0.05	0.08	−0.96
2049.37	Fe III + Mn III	0.00	−0.24	−0.3[a]	0.05	0.2[a]	0.25[a]	0.20	−0.90[b]
2049.66	Mn III	...	(0.34)	−0.3[a]	0.05	0.2[a]	0.25[a]	(0.77)	(0.09)
2051.85	Fe III + Fe IV	−0.20	−0.30	...	0.25	...	...	...	...
2052.25	Fe III	−0.20	−0.25	...	0.13	...	...	0.35	−0.93
2053.51	Fe III	(−0.58)	−0.35	−0.4	(−0.48)	...	0.00	0.10	−0.98
2054.56	Fe III × 3	−0.24	−0.06	−0.4	0.00	0.0	0.25	0.19	−0.84
2055.85	Fe III	...	(0.25)	−0.2[a]	0.08	0.2[a]	...	...	(−0.24)
2056.15	Fe III	(0.29)	0.02	−0.2[a]	0.14	0.2[a]	...	0.32	(−0.50)
2057.93	Fe III	−0.40	−0.23	−0.5[a]	0.00	...	−0.20[a]	−0.03	−0.72
2058.20	Fe III	−0.38	(−0.45)	−0.5[a]	(−0.37)	...	−0.20[a]	0.00	−0.90
2058.55	Fe III + Cr III	0.10	0.00	−0.1	(0.50)	...	(0.70)	0.40	(−0.65)
2059.67	Fe III + Mn III	0.00	0.00	−0.1	0.10	0.0	(0.70)	0.45	−0.99
2063.40	Mn III	...	−0.18	...	−0.01	0.0	−0.20	0.05	...
2065.26	Fe III × 4 + Fe V	...	−0.30	...	−0.10	...	−0.40	−0.10	−0.85
2066.40	Mn III × 2 + Ni III	−0.30	−0.40	−0.2	−0.20	...	−0.35	0.05	−0.90
2068.25	Fe III	(0.60)	0.10	0.2	(0.30)	(0.5)	(0.43)	0.47	−1.00
2069.82	Fe III + Mn III	0.05	−0.20	0.00	−0.4	...	−0.15	0.20	...
2070.56	Fe III	(0.47)	0.00	−0.3	(0.44)	−0.1[a]	(0.89)	(0.55)	−0.79
2070.98	Fe III	−0.35	−0.35	−0.5	−0.19	−0.1[a]	−0.30	−0.12	−0.70
2074.23	Fe III	−0.15	(−0.70)	...	0.12	...	−0.35	0.14	...
2076.31	Fe III	...	(−0.70)	...	−0.09	...	−0.40	0.05	...
Average.....		−0.16	−0.15	−0.2	0.02	0.1	−0.16	0.16	−0.88
1 σ		0.17	0.15	0.2	0.12	0.1	0.23	0.14	0.10

NOTE.—Abundances are determined from spectrum syntheses using the atmospheric parameters in Tables 3 and 4. Dominant features only are identified here. Results that are $\geq 2\,\sigma$ from the mean are enclosed in parentheses and not included in the average. We find a mean iron group abundance of [Fe/H] = −0.06 ± 0.15 for the main-sequence B-type stars in this table. This is expected for solar neighborhood objects and similar to the B-type star results in CL94 and GL92.

[a] The abundances noted are from a blend of more than one feature listed in the table, e.g., all entries marked by the letter "a" are from a single fit to a blend of those features.

[b] The Ekberg 1993 wavelength does not fit the feature in PG 0832+676, although it does fit the features in the other sharp-lined stars.

equivalent widths for the B III λ2065.8 lines in Figure 7 shows that the line strength is nearly constant between 20,000 and 28,000 K and then drops dramatically at higher and lower temperatures. For example, near 30,000 K, an uncertainty of ±2000 K can change the boron equivalent width by ∓50%. From spectrum synthesis this corresponds to Δ log (B/H) = ∓0.4, a substantial uncertainty for only a 5% uncertainty in $T_{\rm eff}$. For this reason, we examine our boron abundances versus temperature in Figure 8; we also include boron abundances from the literature on a homogeneous temperature scale (discussed below). There is no significant trend, but we mark the temperature limits where the B III λ2065.8 line should be the most reliable.

Our LTE boron abundances in Table 4 are corrected for NLTE effects. For this paper, M. Lemke has extended his calculations (described in Cunha et al. 1997) to higher temperatures. The NLTE calculations were carried out for an abundance of 12 + log (B/H) = 2.6. As seen in Figure 9, the NLTE corrections for the B III lines remain small but reverse their sign in the hotter stars. This is because the ground state of B III is overpopulated at the lower temperatures through collisional coupling and ionization processes between B II and B III, and this is the only mechanism that produces B III NLTE effects at these temperatures. But as the temperature increases, the effects of B II on the ground state of B III are reduced. At the same time, the UV radiation field increases and there is a general shift toward B III as the main ionization stage such that photoionization dominates the B III statistical equilibrium. Eventually, this causes the sign reversal in the B III NLTE corrections.

TABLE 7

REPRESENTATIVE IRON GROUP ABUNDANCE UNCERTAINTIES

Parameters	BD +56°576 Δ[M/H]	HD 34078 Δ[M/H]	HD 36591 Δ[M/H]	HD 216916 Δ[M/H]	PG 0832 Δ[M/H]
$\Delta T_{\rm eff} = \pm 750$ K	∓0.01	±0.2	±0.10	±0.01	∓0.04
Δ log $g = \pm 0.1$	±0.02	∓0.1	∓0.01	±0.03	±0.03
$\Delta\xi = \pm 1$ km s^{-1}	∓0.27	∓0.1	∓0.23	∓0.18	∓0.23
$\Delta\xi_{\rm Ma} = \pm 2$ km s^{-1}	±0.09	±0.0	±0.11	±0.11	±0.14
Shift continuum ±1%.....	∓0.07	∓0.1	∓0.07	∓0.08	∓0.07

TABLE 8

BORON ABUNDANCE UNCERTAINTIES

Parameters	BD +56°576 Δ log (B/H)	HD 34078 Δ log (B/H)	HD 36591 Δ log (B/H)	HD 216916 Δ log (B/H)	PG 0832 Δ log (B/H)
$\Delta T_{\rm eff} = \pm 750$ K.....	±0.01	±0.2	±0.05	±0.00	∓0.01
$\Delta \log g = \pm 0.1$.....	±0.03	∓0.1	±0.03	±0.04	±0.05
$\Delta\xi = \pm 1$ km s^{-1}	∓0.03	±0.0	±0.00	±0.02	±0.00
$\Delta\xi_{\rm Ma} = \pm 2$ km s^{-1}	±0.02	±0.0	±0.00	±0.04	±0.01
Shift continuum ±1%.....	∓0.03	∓0.1	∓0.06	∓0.03	∓0.13
$^{11}B = 2^{10}B$.....	−0.02	0.0	−0.06	−0.12	−0.10
$\Delta V_{\rm rad} = \pm 2$ km s^{-1}.....	±0.10	±0.0	±0.07	±0.03	±0.04
($\Delta V_{\rm rad}$ Mn III λ2065.9)[a].....	(∓0.10)	(±0.0)	(∓0.13)	(∓0.26)	(∓0.00)

NOTE.—ΔB was determined by scaling the Mn III λ2065.9 line abundance a priori according to the results listed for the five uncertainties examined for the iron group elements in Table 7. We also examine a smaller $^{11}B/^{10}B$ ratio since this may be affected by rotational mixing (discussed in § 4).

[a] Changing the radial velocity required a completely new fit, thus the new "best" Mn III λ2065.9 abundance is also listed here.

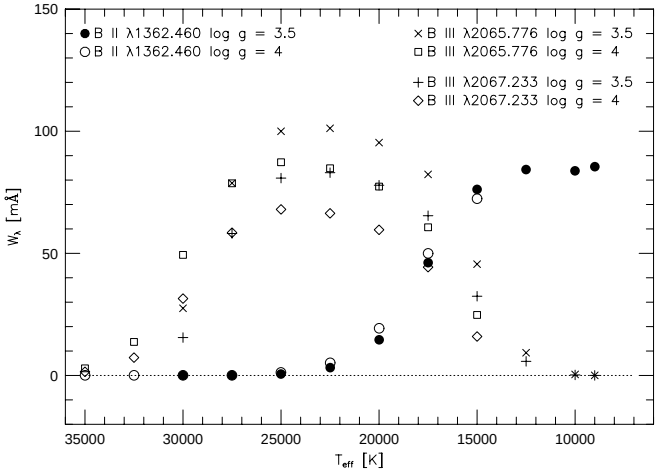

FIG. 7.—Predicted equivalent widths for boron lines in B-type stars, from NLTE calculations. The B III λ2065.8 line strength plateaus between 18,000 and 29,000 K. At hotter temperatures, an increase in $T_{\rm eff}$ of only 5% reduces the predicted equivalent width by 50%, or 0.4 dex in the boron abundance.

Boron is clearly present and undepleted in only two stars in our sample: BD +56°576 and HD 216916. That the boron abundance is quite different in stars of very similar atmospheric parameters is obvious from inspection of the spectra of HD 216916 and HD 16582. For example, compare the large differences in the B III–Mn III λ2066 blend in Figure 4 for these two stars with insignificant differences in their other features (see also Figs. 1, 2, and 3). In addition, both of these stars are β Cep variables (see Table 2), thus we conclude that the β Cep variability mechanism is not a cause of surface mixing. Similarly, the Orion star HD 36591 has similar atmospheric parameters to another Orion star, HD 35299, yet vastly different boron line strengths are seen in Figure 6.

Six of our stars have *IUE* spectra that were examined by PQ01. Owing to the lower S/N and resolution of *IUE* spectra, their boron abundances are less precise than ours. When boron is strong, as in HD 216916, our results are in excellent agreement and with similar uncertainties (±0.2

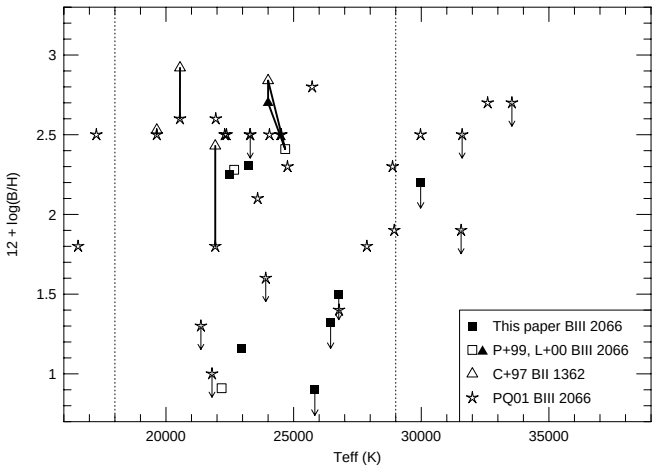

FIG. 8.—Boron abundances vs. temperature. Temperatures from GL92 have been reduced by 3.4% (see text). This plot shows that there is no significant trend in the B III λ2065.8 abundances, although we note the upper and lower temperature limits where the B III λ2065.8 line yields the most reliable abundances. Thick lines connect boron abundances found for the same stars from different analyses.

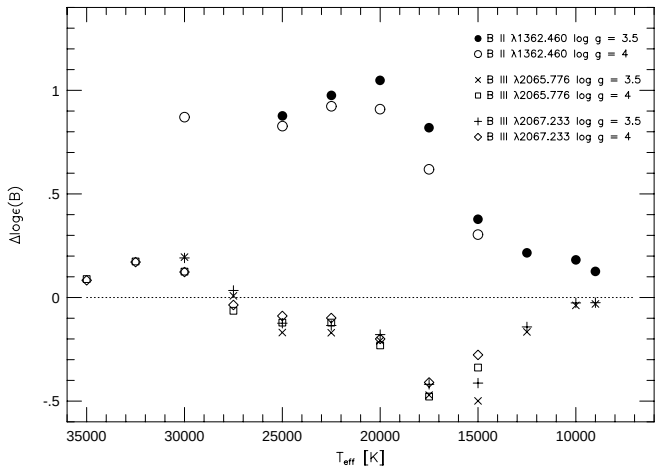

FIG. 9.—NLTE corrections to UV boron lines. These calculations are identical to those discussed in Cunha et al. (1997); here we extended the grid to hotter temperatures (35,000 K) for the B III features. The change in orientation of the B III NLTE correction in the hotter models appears to be due to the much weakened boron lines being dominated by overionization effects (as opposed to line transition rates, which dominate at lower temperatures).

dex). On the other hand, PQ01 report detecting the boron line in HD 34078, which we do not confirm (see Fig. 5). For the other four stars in common, we report significantly lower abundances (HD 16582) or lower upper limits.

4. DISCUSSION

4.1. *The Initial Abundance of Boron*

In order to pursue our principal goal of testing predictions of boron depletion due to rotationally induced mixing, it is necessary to establish the initial boron abundance of these local B-type stars. (PG 0832+676 is discussed separately.) We suppose that the highest boron abundances across our sample and others provide a close approximation to the initial boron abundance. We further assume that stellar boron abundances that are substantially less than the presumed initial abundance do not reflect an unusually low initial value but rather arise from internal processes that deplete boron.

The mean NLTE boron abundance from BD +56°576 and HD 216916 is $12 + \log (B/H) = 2.3$. The Proffitt et al. (1999) analysis of another two stars gives $12 + \log (B/H) = 2.4$ (considering NLTE corrections), and the mean NLTE abundance of stars with boron detections from the sample considered by PQ01 gives $12 + \log (B/H) = 2.4$. Cunha et al. (1997) found near-solar boron abundances from two B-type stars in the Orion OBIc subassociation, although those results were from the B II λ1362 line. Boron from the B I λ2497 line in F–G main-sequence stars, with $-0.15 \leq [Fe/H] \leq 0.15$, is $12 + \log (B/H) = 2.6$ from Cunha et al. (2000a).

These stellar abundances should be closely related to the IS abundance of boron, as standard evolutionary models, as well as those including rotational effects (see below), predict survival of surface boron through the pre–main-sequence phase. Boron is detected in IS diffuse clouds by the B II λ1362 resonance line (Jura et al. 1996; Lambert et al. 1998; Howk, Sembach, & Savage 2000). The lower limit to the IS abundance, $12 + \log (B/H) \geq 2.4$ suggested by Howk et al. (2000), is consistent with the above stellar abundances. The lower limit is given in recognition of the possibility that boron may be depleted onto IS grains. It is most unlikely that boron is present *in* grains, if, as is widely supposed, grains are formed primarily in stellar outflows from red giants whose outer envelopes will be highly depleted in boron.

These stellar and nebular abundances are slightly lower than the solar system (meteoritic) value of $12 + \log (B/H) = 2.78$ (Zhai & Shaw 1994). For the B-type stars and the IS gas, this reduction is in line with similar underabundances (relative to the Sun) for oxygen and other light elements. Since our primary interest lies in the B-type stars depleted in boron by an order of magnitude or more, the difference between an initial boron abundance of 2.4 and 2.8 is largely irrelevant.

It is also worth investigating the boron abundance in the Orion association as a fiducial point, since there are both stellar and IS determinations available. In general, $2.4 \leq 12 + \log (B/H) \leq 2.9$ from B-type stars and IS sight lines (among the references above). Some stars in Orion show large boron depletions though. Two of our stars are or were members of the Orion association: HD 36591 belongs to the Ib subgroup, and HD 34078 (AE Aur) is a well-known runaway star. Neither star shows a detectable B III line. While the boron depletion in HD 34078 might be related to its transformation as a runaway star (e.g., contamination of the star by ejecta from its exploding companion), HD 36591's low boron abundance is plausibly identified as arising from internal effects (discussed below). This result is significantly different from other boron determinations from B-type stars in Orion (Cunha et al. 1997; Proffitt et al. 1999; Lemke, Cunha, & Lambert 2000).

Low boron abundances have been found in some other stars in Orion. Cunha, Smith, & Lambert (1999) and Cunha et al. (2000b) determined the boron abundances in three G-type stars in Orion from the B I λ2497 line. One of these, BD −5°1317, resulted in an abundance 5 times less than solar, $12 + \log (B/H) = 2.1 \pm 0.2$. Surprisingly, this star also proved to be oxygen rich (Cunha, Smith, & Lambert 1998), 3 times larger than the Orion nebular abundance (Esteban et al. 1998). These results lead Cunha et al. (2000b) to propose a boron-oxygen anticorrelation, possibly the result of dilution of IS boron by relatively boron-poor but oxygen-rich ejecta from recent Type II supernovae.

PQ01 also discovered severely boron-depleted B-type stars, which muddles the issue of a boron-oxygen anticorrelation, particularly as the boron depletions are not related to oxygen enrichment. In Figure 10 (*left panel*), we show the boron-oxygen anticorrelation from published data for Orion, as well as our star HD 36591. (We note that PQ01 include seven more Orion stars with depleted boron; however, five are hot stars like HD 34078, which we consider less reliable boron abundance indicators, and two have no published oxygen abundances.) In the right panel, we include only stars where boron is determined from the reliable B III feature (the boron and oxygen abundances plotted are from Table 9, which is discussed further below). The existence of a boron-oxygen anticorrelation is not obvious from the B III data alone, although we note that much of the B III data are from lower quality *IUE* spectra.

The phenomenon of boron depletion is not confined to the Orion association. Proffitt et al. (1999) found that the field star HD 3360 is boron depleted, and we have found

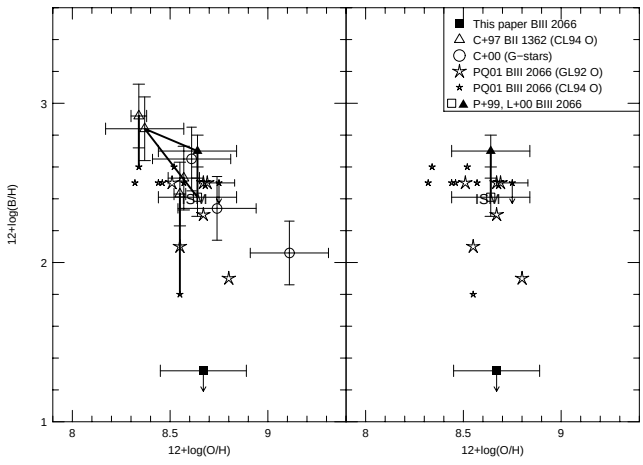

FIG. 10.—Boron vs. oxygen abundances in Orion stars. Left panel shows all stars with both boron and oxygen abundances, including B-type and G-type stars, and the IS abundances. Left panel also shows the effect of replacing B II abundances with those from the B III feature (*thick lines*). Right panel shows only the B III abundances in B-type stars. The B III abundances do *not* confirm the B-O anticorrelation (see text for further discussion), although the PQ01 *IUE* data points have large uncertainties that are not shown for clarity.

TABLE 9

NLTE Boron and CNO Abundances in B-Type Stars

Star	Literature				Reference	Corrected				$T_{\rm eff}$
	B	C	N	O		B	C	N	O	
This Paper										
BD +56°576.....	...	7.89	7.35	8.57	1	2.25[a]	7.84	7.62	8.34	22500
HD 16582.....	≤1.3	8.14	8.12	...	2, 3	1.16[a]	8.15	8.10	...	22942
HD 36591.....	...	8.24	7.64	8.64	3	≤1.32[a]	8.25	7.69	8.67	26449
	≤2.0	8.25	7.58	8.60	2, 4	...	8.32	7.64	8.54	26330
HD 50707.....	≤1.7	8.20	8.23	8.87	2, 3	≤1.5[a]	8.21	8.29	8.89	26768
HD 205021.....	≤1.2	7.96	7.97	8.77	2, 3	≤0.9[a]	7.98	8.00	8.81	25831
HD 216916.....	2.4	8.15	7.66	8.64	2, 3	2.31[a]	8.17	7.64	8.61	23232
GHRS Boron										
HD 886.....	2.2	8.41	7.78	...	2, 3	2.2	8.40	7.75	...	21899
	2.29[b]	...	...	...	5	2.28[b]	...	...	...	22670
HD 3360	≤1.2	8.43	8.26	...	2, 3	≤1.2	8.40	8.22	...	21426
	0.92[b]	...	...	...	5	0.91[b]	...	...	...	22180
HD 35299.....	2.9	8.17	7.71	8.63	2, 3	2.9	8.19	7.70	8.64	23831
	2.7	8.38	7.74	8.57	4, 6	2.7	8.40	7.67	8.37	24000
	2.46[b]	...	...	...	5	2.41[b]	...	...	...	24670
	2.84[c]	...	...	...	7	2.84[c]	...	...	...	24000
HD 35039.....	2.6	8.40	7.76	...	2, 3	2.6	8.35	7.70	...	20547
	2.92[c]	8.50	7.85	8.60	4, 7	2.92[c]	8.36	7.65	8.34	20550
HD 36285.....	2.43[c]	8.57	7.95	8.80	4, 7	2.43[c]	8.48	7.77	8.55	21930
	1.8	...	...	...	2	1.8	...	...	...	22230[d]
HD 36430.....	2.53[c]	8.54	7.89	8.84	4, 7	2.53[c]	8.38	7.67	8.57	19640
	2.5	...	...	...	2	2.5	...	...	...	19640
***IUE* Boron**										
HD 22951.....	1.8	8.14	7.69	8.45	2, 3	1.8	8.11	7.69	8.42	27869
HD 29248.....	2.5	8.25	7.75	8.70	2, 3	2.5	8.27	7.74	8.67	23290
HD 30836.....	...	8.44	7.79	...	3	...	8.41	7.75	...	21368
	≤1.3	...	...	...	2	≤1.3	...	...	...	20819[d]
HD 34816.....	2.3	8.26	7.66	8.75	2, 3	2.3	8.17	7.59	8.67	28875
HD 35337.....	2.1	8.29	7.65	8.56	2, 3	2.1	8.31	7.64	8.55	23590
HD 35468.....	≤1.0	8.30	8.13	...	2, 3	≤1.0	8.28	8.09	...	21803
HD 36351.....	2.6	8.35	7.83	8.76	2, 4	2.6	8.28	7.68	8.52	21950
HD 36629.....	2.5	8.38	7.75	8.55	2, 4	2.5	8.32	7.61	8.32	22300
HD 36959.....	...	8.10	7.76	8.65	3	...	8.13	7.76	8.69	24517
	2.5	8.33	7.76	8.76	2, 4	2.5	8.37	7.73	8.61	24890
HD 36960.....	...	8.27	7.72	8.88	3	...	8.18	7.65	8.80	28941
	1.9	8.36	7.50	8.72	2, 4	1.9	8.39	7.54	8.71	28920
HD 37209.....	...	8.17	7.57	8.50	3	...	8.19	7.56	8.51	24053
	2.5	8.27	7.63	8.83	2, 4	2.5	8.29	7.55	8.63	24050
HD 37356.....	2.5	8.46	7.84	8.67	2, 4	2.5	8.41	7.70	8.44	22370
HD 37481.....	≤2.5	8.40	7.65	8.96	2, 4	≤2.5	8.39	7.55	8.75	23300
HD 37744.....	2.5	8.34	7.85	8.63	2, 4	2.5	8.37	7.80	8.46	24480
HD 41753.....	2.5	8.58	8.15	...	2, 3	2.5	8.53	8.10	...	17272
HD 44743.....	2.8	8.21	7.71	8.75	2, 3	2.8	8.23	7.73	8.78	25725
HD 46328.....	≤1.4	8.04	7.89	8.69	2, 3	≤1.4	8.05	7.95	8.71	26778
HD 52089.....	≤1.6	8.25	8.12	8.50	2, 3	≤1.6	8.27	8.04	8.30	23908
HD 184171.....	1.8	8.32	7.91	...	2, 3	1.8	8.28	7.86	...	16557
HD 214993.....	2.3	8.25	7.80	8.78	2, 3	2.3	8.28	7.82	8.83	24759

Note.—This table summarizes the NLTE B, C, N, and O data for B-type main-sequence stars, excluding stars with 18,000 ≤ $T_{\rm eff}$ ≤ 29,000 K (see text). The left side of the table quotes NLTE abundances as published in the literature. The right side of the table corrects the NLTE CNO abundances by (1) including adjustments to correct for the use of Gold, instead of Kurucz, model atmospheres; and (2) reducing the GL92 temperatures by 3.4% and adjusting their abundances according to the offsets listed in their Table 9. This reduction in the GL92 temperatures has a negligible effect on the B III abundances (see, e.g., Table 8). There are some significant differences between the GL92 and CL94 abundances for the five stars in common. The differences in oxygen appear to be due to differences in ξ, whereas those in C appear when two strong C III lines are included by GL92. N is in good agreement throughout, with the only significant difference of ∼0.1 dex occurring for the hot star HD 36960.

[a] Boron abundances from this paper.

[b] Proffitt et al. 1999 LTE B III abundances have been NLTE corrected (corrections are from this paper; see Table 8). On the right side, their abundances are also corrected for the differences between their temperatures and the reduced GL92 temperatures listed (small effect).

[c] Boron from B II λ1362.5, which is severely blended with metal lines.

[d] PQ01 temperatures are the same as CL94, or they have adopted GL92—820 K. This offset is very similar to our reduction of 3.4%. We note when the PQ01 and GL92 temperatures differ by more than 250 K.

References.—(1) Vrancken et al. 2000. (2) PQ01. (3) GL92. (4) CL94. (5) Proffitt et al. 1999. (6) Lemke et al. 2000. (7) Cunha et al. 1999.

several boron-depleted stars in other OB associations, as did PQ01. Fliegner et al. (1996) first proposed that boron depletions may result from rotationally induced mixing during the main-sequence lifetime of B-type stars. We discuss this in the next section.

4.2. *Rotationally Induced Mixing*

Recent models by Heger, Langer, & Woosley (2000) follow the evolution of the angular momentum distribution and the occurrence of associated mixing processes in massive stars from the pre–main sequence through core collapse. They find that rotational mixing can affect stellar surface abundances, stellar lifetimes, and the evolution of a star across the H-R diagram (HL00). These new models have fundamental consequences for the age determination of young stellar clusters, and they can reconcile the long-standing mass discrepancy problem (that spectroscopic masses differ from those inferred from stellar evolution tracks; Herrero et al. 1992).

In general, a rotating star has a lower effective gravity, thus it acts like it has less mass at core H ignition. Later, during core H burning, rotationally induced mixing of protons from the envelope into the convective core and of helium from the core into the envelope will lead to higher luminosities compared to nonrotating models. In addition, the effective temperature is lower, thus the zero-age main-sequence (ZAMS) position on the H-R diagram changes from a nonrotating model. Evolution on the main sequence then depends on the star's mass and rotation rate, as well as the efficiency of mixing in the upper convective core and stellar interior.

HL00's models cover a mass range of 8–25 $M_{\odot}$ and a range of rotational velocities from 0 to $\sim$450 km s^{-1}. They computed two sets of models, with different assumptions on the efficiency of rotational mixing in layers containing a gradient in the mean molecular weight μ (called a μ-barrier). In one set, the μ-barriers are ignored, and the overall efficiency of rotational mixing had to be reduced in order to meet observational constraints. In the other set, μ-barriers are taken into account, and again the overall mixing efficiency above the μ-barrier is set by observational constraints (see Heger et al. 2000 for details). The differences between the two sets of models reflect the remaining uncertainties in the theoretical description of the rotational mixing processes. Finally, it is interesting to note that even though the rotationally induced μ-barrier *inhibits* mixing just above the core, the current models show that the envelope above the μ-barrier is very well mixed, thus CN-processed gas is *more* evident up through the photosphere than when the μ-barrier is ignored.

The range in velocities examined by the models is thought to be typical for B-type stars. For example, Fukuda's (1982) statistical study of rotational velocities found B2 V and B2 IV stars with mean v sin i values of 154 and 110 km s^{-1}, respectively, and that OB stars generally span a range in v sin i of 100–400 km s^{-1}. In addition, de Jager (1980) summarizes mean equatorial velocities for B1/B2 V stars (the majority of stars in this paper) as $\sim$200 km s^{-1}. Although all the stars in this paper, and others with good abundance analyses, are sharp-lined objects, the usual assumption is that many of these stars are (near) pole-on rotators.

In Figure 11 we show the HL00 models for 0 and 200 km s^{-1}, with and without μ-barrier effects in the log g–log $T_{\rm eff}$ diagram. We also include our stellar targets, and more B-type stars with boron and CNO abundances from the literature, to show their approximate mass range and main-sequence ages (differences between the symbols are discussed below). We notice that the model ZAMS is offset from the highest gravity stars. This is most likely an artifact of uncertainties in the temperature scale (discussed below), which subsequently affects the determinations of gravity and ξ.

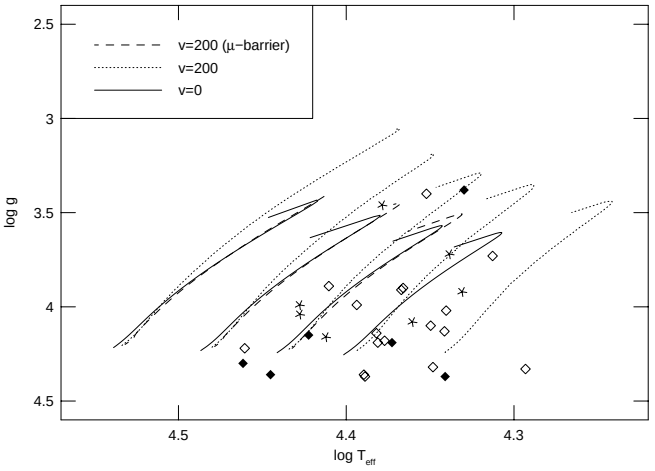

FIG. 11.—Gravity vs. $T_{\rm eff}$ for B-type main-sequence stars in Table 9. Open diamonds mark normal stars ($B > 2.2$ and $N \leq 7.8$), filled diamonds show boron-depleted stars ($B \leq 2.2$ and $N \leq 7.8$), and asterisks denote the N-rich stars ($B \leq 2.2$ and $N > 7.8$). Evolution tracks are from HL00 for stars of 8, 10, 12, 15, and 20 $M_{\odot}$, two rotation rates, and considering μ-barrier effects, through the H core burning phase. This plot shows the mass and age range of the B-type stars examined in this paper, as well as the distribution of boron depletions and nitrogen enrichments on the main sequence.

4.2.1. *Boron versus Nitrogen: Predictions*

HL00's models can reproduce previously unexplained observations of massive stars (e.g., various abundance anomalies), and the models make certain predictions (see their discussion of the observational evidence and testable predictions). The prediction that concerns us in this paper is the relationship between boron and nitrogen[4] during main-sequence evolution.

Mechanisms that can deplete boron at the surface of stars can also enrich the surface in the products of the CN cycle: material that is rich in nitrogen and depleted of carbon, yet where the sum C + N is preserved. Extremely deep mixing could also bring ON-cycled material to the surface, preserving the sum C + N + O. Thus, in Figure 12 we show the boron-nitrogen relationship and the rate of boron depletion predicted by various HL00 models for main-sequence evolution (through core H burning). We show models that include μ-barrier effects for 12 $M_{\odot}$ at five rotational velocities, and for comparison we have included two 15 $M_{\odot}$ models at 200 and 450 km s^{-1} as well as the 10 and 15 $M_{\odot}$ models without the μ-barrier effects. These figures allow us to examine the effects due to rotation rate, mass, age, and mixing efficiencies.

[4] We note that boron vs. the ratio N/C is also a good indicator, but our opinion is that the small depletions in carbon due to mixing do not clearly compensate for the added uncertainties in the B-type star carbon abundances.

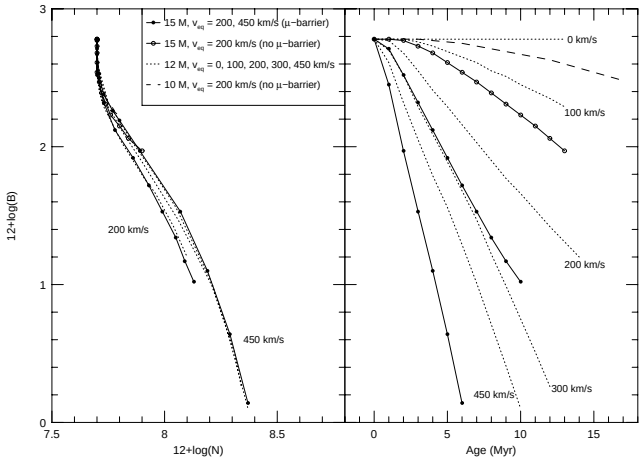

FIG. 12.—Predictions of boron vs. nitrogen (*left panel*) and boron vs. main-sequence age (*right panel*) from the rotating stellar evolution models from HL00. Predictions for a 12 $M_\odot$ model with five rotational velocities are shown (*dotted lines*; velocities are marked in the right panel). For comparison, predictions for a 15 $M_\odot$ model with rotational velocities of 200 and 450 km s^{-1} are shown (*solid lines*). Additionally, 10 and 15 $M_\odot$ models, rotating at 200 km s^{-1} and which ignore the effects of μ-barriers, are shown. In the left panel, it is striking that the boron-nitrogen relationship is nearly the same for various masses, rotation rates, and efficiency of mixing with/without μ-barriers, although some tracks end before significant abundance changes. However, in the right panel, it can be seen that the rate of boron depletion is sensitive to these parameters.

One of the most interesting results is that the boron-nitrogen relationship is nearly the same for all models. This occurs because boron is destroyed throughout most of the star very early in its main-sequence lifetime ($\leq 10^4$ yr). Only the outermost layers of the stellar interior are cool enough to retain the initial boron (the outer ~ 1 $M_\odot$ for 10–20 $M_\odot$ stars). Meanwhile during this early ZAMS phase, the CN cycle begins in the core, transforms carbon into nitrogen, and mixes this gas into the interior through convective overshoot and/or semiconvection. As the star ages on the main sequence, rotation will mix the CN-cycled gas up through the stellar interior, while also mixing the pristine outer layers downward. Figure 12 illustrates that mixing the radiative envelope of a massive main-sequence star will always have the same consequences for the surface abundances: boron is depleted first, and nitrogen is enriched only later (also shown in Fliegner et al. 1996). Because of the similarity in the structure of the envelopes of the stars considered, in particular the shallowness of the surface layer that contains pristine boron and the depth of the layers where nitrogen is enriched, the same abundance changes are predicted independent of all parameters.

On the other hand, the *timescales* for the B-N abundance changes do differ significantly between the models. Since rotational mixing is less effective for slower rotation rates or lower masses, the abundance changes simply take longer to occur. Furthermore, very few models predict high N/C ratios at the end of the main-sequence lifetime, thus additional processing/mixing after the main-sequence phase (such as the first dredge-up) can be examined through the N/C ratios of more evolved stars.

We comment once again that mass loss could produce the same B-N abundance changes as rotation (having the same ZAMS starting conditions as well). However, the mass-loss rates for B-type stars are much smaller than required (as discussed earlier), thus favoring rotation for this phenomenon. In addition, boron depletion and nitrogen enrichment are predicted by mass transfer in a close binary system. Wellstein (2000) and Wellstein et al. (2001) predict changes in surface abundances of boron and CNO due to the transfer of nuclear processed matter. The current models predict much larger boron depletions though, and there is always a very strong CNO signature as well. Therefore, the existence of moderately boron-depleted stars without nitrogen enrichments is a unique signature of rotational mixing effects.

4.2.2. *Boron versus Nitrogen: Observations*

In the abundance analysis described above, we have adopted the GL92 atmospheric parameters. Systematic differences between GL92 and other B-type star analyses suggest that this temperature scale is too hot (e.g., Korotin, Andrievsky, & Luck 1999; CL94). In fact, GL92 did increase their temperature scale by 3.4% from the photometric determinations. This increase removed an unexpected relationship between NLTE CNO abundances and temperature. However, this relationship appears to have been due to the NLTE CNO abundances having been determined from Gold (1984) model atmospheres, instead of the more heavily line-blanketed Kurucz models.

In Table 9 we have reduced the GL92 temperature scale by 3.4% and applied their NLTE CNO abundance corrections listed in their Table 9 (their Δ values). We have also applied a correction to account for the Gold-Kurucz offsets, as tabulated by CL94 (their Table 10). (Note that the latter correction is derived from differences in LTE abundances between Gold and Kurucz models, and we assume that the same will apply to the NLTE abundances, an assumption that should be checked.) The GL92 temperatures are now in good agreement with CL94 values for stars in common. In the case of BD $+56°576$, which was not analyzed by GL92 or CL94, we take the parameters and NLTE CNO results of Vrancken et al. (2000) but add 0.4 dex to their published nitrogen value to account for the systematic differences they discuss between their analysis and those by GL92 and Kilian (1992, 1994).

The GL92 NLTE nitrogen abundances are now in excellent agreement with CL94 values for stars in common. Only the hottest star, HD 36960, shows a nonnegligible nitrogen difference of ~ 0.1 dex. However, it is surprising that the carbon and oxygen abundances often differ between these analyses, by up to 0.25 dex. For carbon, the abundances differ when GL92 include two strong C III lines. For oxygen, the differences are traceable to the adopted ξ values. CL94 adopt higher ξ values as their analysis is more sensitive to ξ as a result of some stronger lines. For consistency, we adopt the corrected GL92 values for CNO in Table 9 whenever possible.

The boron abundances determined from the B III feature are not sensitive to these uncertainties in temperature, except for the hottest and coolest stars that we consider less reliable boron indicators (discussed above), and thus that we have excluded from Table 9 (including our hot target HD 34078). We also note that the uncertainties in $T_{\rm eff}$ and/or gravity do not significantly affect the boron-nitrogen relationship that we seek, i.e., the B III and N II line abundances react similarly to the atmospheric parameters in most cases (only in the coolest stars is nitrogen more sensitive to the atmospheric parameters). Thus, uncertainties in the parameters cannot induce a B-N anticorrelation.

4.2.3. *Predictions versus Observations*

To compare the boron and nitrogen abundances in B-type stars to the model predictions, we have gathered abundances from this analysis and the literature, corrected them to be on a homogeneous temperature scale, and applied the known Gold-Kurucz model atmosphere abundance corrections (discussed above). We have also limited the atmospheric parameter range of our sample to $18{,}000 \leq T_{\rm eff} \leq 29{,}000$ K, where the B III line strength is in a plateau, and $\log g \geq 3.4$ to examine main-sequence stars only. GL92 showed that their sample of B-type stars contained some stars mildly depleted of carbon and enriched in nitrogen with no measurable spread in the oxygen abundances. The C-N signature is indicative of CN-cycled material in the atmospheres of some stars. There is no evidence for ON-cycled gas in main-sequence B-type stars.

In Figure 13 we can see that most stars gather around the point $12 + \log({\rm B/H}) = 2.6$ and $12 + \log({\rm N/H}) = 7.7$, consistent with the ISM boron abundance in Orion (discussed above) and the ISM nitrogen abundance [e.g., $12 + \log({\rm N/H}) = 7.8$; Esteban et al. 1998]. Possibly, there is a small intrinsic spread (initial boron may be higher [about 2.8] and initial nitrogen lower [about 7.6]), or perhaps some small depletion by rotation has already occurred. Boron and nitrogen predictions from HL00 for the 12 $M_\odot$ models (with 200 km s^{-1} and μ-barrier effects) are shown in Figure 13. The same model is shown scaled with three different initial boron and nitrogen abundances (all initial abundances used here are within the observational uncertainties) to better compare to the stellar observations. Only the predicted ^{11}B abundances are traced. It is unclear whether the isotope ^{10}B is more or less readily destroyed by protons as a result of uncertainties in the ^{10}B(p, α) thermonuclear reaction rate (i.e., Thielemann et al. 1995 REACLIB95 rates[5] vs. Angulo et al. 1999 NACRE rates) and thus whether the ^{11}B/^{10}B ratio would increase or decrease in regions of partial boron destruction. The HL00 models predict a slower depletion rate for ^{10}B, having adopted the Thielemann et al. (1995) reaction rates; thus, ^{11}B/^{10}B = 4 adopted for the ZAMS is predicted to reduce to $\sim$2 in the stellar envelope by the end of the main-sequence lifetime. We note that differences in the boron isotopic ratio have a negligible effect on the boron abundance determinations in most stars though (see Table 8).

Only two stars have low-boron *determinations*, HD 16582 (this paper) and HD 3360 (Proffitt et al. 1999). Several others have interesting upper limits that follow the boron-nitrogen trend predicted by the rotating models. HD 36591 in Orion is particularly interesting since it shows a strong boron depletion with no enrichment in nitrogen; the model predictions are most consistent with this star for the lowest initial nitrogen (= 7.6) abundance.

In Figure 14 we examine the boron abundances with stellar age. Three stars in this paper are in young clusters and show boron depletions that are fitted well by rotating model predictions. Two of these stars have nitrogen enrichments, thus they could also be explained by binary accretion (although only one is in a known binary system), but the third has unenriched nitrogen. As previously stated, the best interpretation for boron depletion without nitrogen enrichment is rotational mixing. This third star is HD 36591, again, and we find that the most extreme models, e.g., 20 $M_\odot$, $v_{\rm eq} = 450$ km s^{-1}, reproduce its age, boron, and nitrogen abundances well. Unfortunately, the atmospheric parameters for this star make it very unlikely that it is a 20 $M_\odot$ star (see Fig. 11). Perhaps mixing efficiencies above μ-barriers can be higher than currently predicted.

Also seen in Figure 14 is that some B-type stars in older clusters have normal boron abundances. There are two possibilities for this. First, they may be true slow rotators (not

[5] Available on-line at http://ie.lbl.gov/astro/friedel.html.

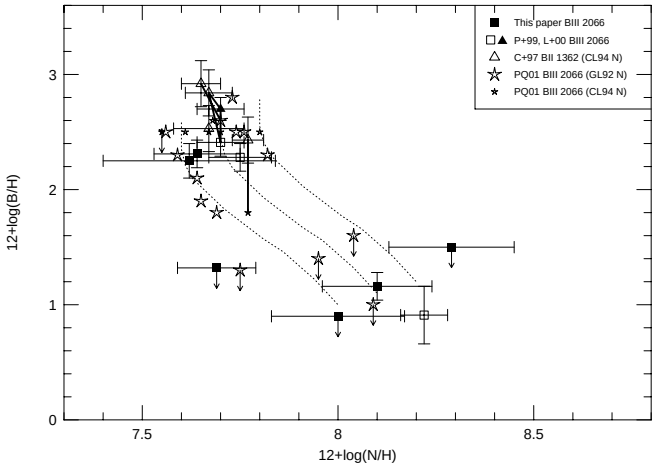

FIG. 13.—Boron vs. nitrogen in main-sequence B-type stars, with predictions for the 12 $M_\odot$ models at 200 km s^{-1} through the H core burning phase, and three sets of initial abundances [$(B_i, N_i) = (2.6, 7.6)$, (2.8, 7.7), and (2.8, 7.8), all within range of the IS and ZAMS stellar abundances]. The stellar abundances plotted are those listed in Table 9. Thick lines connect boron abundances for the same stars from different analyses. The observations are in good agreement with the predictions, suggesting that rotational mixing is significant on the main sequence in some B-type stars.

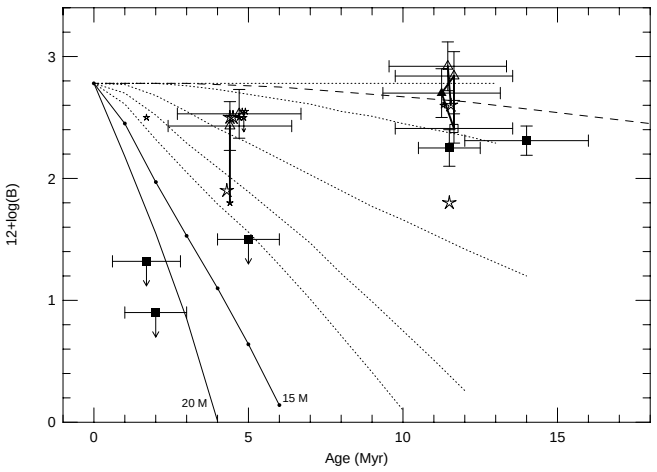

FIG. 14.—Boron vs. cluster ages (see Table 2 for ages and references) for B-type stars in associations. Stellar data symbols are the same as in Fig. 13. Tracks are the same as in Fig. 12 (some tracks are not shown here for clarity). One additional track is included to show the predictions for a 20 $M_\odot$ star with μ-barrier effects, rotating at 450 km s^{-1} (*solid line*). Three boron-depleted young stars (HD 36591, HD 50707, HD 205021) are fitted well by the rotating model predictions, although the most boron-depleted stars are best fitted by the rapidly rotating 20 $M_\odot$ model, which is likely too massive for these stars (see Fig. 11). Many of the older stars in this sample that do not show boron depletions are less massive (e.g., the 10 $M_\odot$ track fits them well; *dashed line*), though some are likely to be true slow rotators as well.

rapidly rotating stars seen pole-on as is usually assumed for sharp-lined objects). This is likely true for some stars, e.g., HD 216916 is an eclipsing binary (Pigulski & Jerzykiewicz 1988), thus its low $v \sin i$ is probably close to its equatorial velocity. In addition, some older subgroups of OB associations have been reported to have an excess of slow rotators (Guthrie 1984; see also the discussion by Grebel, Richtler, & de Boer 1992). Second, some stars may be lower mass objects, e.g., the 10 $M_\odot$ models require more time to mix hotter gas from the interior to the surface, thus nitrogen and boron remain near their initial abundances longer. Schoenberner & Harmanec (1995) determined masses of main-sequence B-type stars in binary systems and found that stars in our primary temperature range (24,000–28,000 K) have masses of 10–12 $M_\odot$, consistent with Figure 11.

In Figure 11 we also examine the boron (from B III only) and nitrogen abundances on a $T_{\rm eff}$-gravity diagram to examine the abundance distributions across the main sequence. The stellar data are divided into three groups: normal stars ($B > 2.2$ and $N \leq 7.8$), boron-depleted stars ($B \leq 2.2$ and $N \leq 7.8$), and nitrogen-rich stars ($B \leq 2.2$ and $N > 7.8$). As expected, there are no N-rich and B-normal stars. Evolution tracks from HL00 are shown for 8–20 $M_\odot$ through the core H burning phase. In general, the three groups of stars have the same range in $T_{\rm eff}$ and gravity, and thus in age and mass, suggesting that their differences are due to another parameter, like rotation rate. It is interesting that most of the B-depleted/N-normal stars are near the ZAMS, as is predicted for rapid rotators. In addition, one might argue that among the most massive stars, more of them show B depletions; this would be consistent with the models if the rotation rates are similar throughout.

Finally, it is pleasing that BD $+56^\circ 576$, the star with the lowest surface gravity of our sample, has apparently retained its initial complement of boron and has unenriched nitrogen. This star is in an eclipsing binary system, which implies that its $v \sin i$ value is very close to its current rotational velocity. Thus, BD $+56^\circ 576$ is probably a slow rotator today and was probably a slow rotator on the ZAMS (although it may have spun down somewhat from its ZAMS rotation rate). Only one other star shows unenriched nitrogen and a lower surface gravity, HD 30836, but PQ01 show that this star has depleted boron, suggestive of rotational mixing. (This star is in Ori OB1, but it is not in Fig. 14 since its subassociation, thus age, is not clear.)

4.3. *PG 0832+676*

Our determination of the metallicity of PG 0832+676 is [Fe/H] = -0.88 ± 0.10, which compares with [Fe/H] = -0.51 given by Hambly et al. (1996) from a single optical Fe III line in a differential analysis with respect to the Galactic B-type star HR 1886. Combining our [Fe/H] with the mean α-element (Mg, Si, and S) abundance from Hambly et al. (1996), we obtain [α/Fe] = 0.5, which is the expected value for a star of this metallicity to within the errors of measurement (e.g., [O/Fe] = 0.3 for [Fe/H] = -0.9, as for the mildly metal-poor clusters M4 and M71; Ivans et al. 1999; Sneden et al. 1992; although the O/Fe ratio in metal-poor stars is currently controversial; cf. Lambert 2000).

Relative to [Fe/H] = -0.88, PG 0832+676 is enriched in carbon, nitrogen, and oxygen, according to the Hambly et al. (1996) results: [C/Fe] $\simeq$ [N/Fe] $\simeq$ [O/Fe] $\simeq$ 0.7–0.8. This O/Fe ratio is somewhat larger than expected for a normal metal-poor star in the halo (see α/Fe ratio comments above), and carbon and nitrogen appear enriched relative to normal stars. These results are consistent with the identification of PG 0832+676 as a post-AGB star with carbon and oxygen added in the AGB phase and nitrogen enhanced by the earlier first dredge-up. Certainly this scenario is consistent with our nondetection of boron. Our limit of $12 + \log (\rm B/H) \leq 0.60$ is much less than the expected initial abundance of $12 + \log (\rm B/H) = 1.9$ at [Fe/H] = -0.9 (based on the analysis of 14 cool dwarfs by Cunha et al. 2000a).

Thus, in summary, the chemical pattern in PG 0832+676, low [Fe/H], high [α/Fe] and [CNO/Fe], and very low [B/H], suggests that this star is a post-AGB star, in agreement with the conclusion by Hambly et al. (1996) that PG 0832+676 is a highly evolved star.

5. CONCLUSIONS

Boron in hot stars, like lithium in cool stars, is shown to be a tracer of some of the various processes affecting a star's surface composition that are not included in the standard models of stellar evolution. If the initial boron abundances of local hot stars are similar from star to star and association to association, then the large spread in boron abundances, a factor of at least 30 across our sample, shows that boron abundances are a clue to unraveling the nonstandard processes that affect young hot stars. In this paper we have focused on the role of rotationally induced mixing.

Models of stars with masses near 10 $M_\odot$ (HL00) show that rotationally induced mixing during main-sequence evolution can reduce the surface boron abundance and increase surface nitrogen. A signature of rotationally induced mixing is that the initial decline of boron precedes an observable change in nitrogen. The correlation between the decline of boron and the rise in nitrogen is almost independent of rotational velocity and mass of the star. On the other hand, the extent and rate of change of the abundances are dependent on both velocity and mass (Fig. 12).

Our results confirm the discovery by Proffitt et al. (1999) that boron may be quite severely depleted in otherwise normal B-type stars: six of the eight stars in our program show a reduced boron abundance. That boron depletions are not a rare occurrence is consistent with PQ01's survey of *IUE* spectra. Boron depletions are attributed to rotationally induced mixing (although N-rich stars could also be explained by binary mass transfer). The correlation between the boron and nitrogen abundances follows the predicted trend quite well (Fig. 13).

Our use of stars from various OB associations allows us to investigate the rate of change of the surface abundances. Stars showing a normal boron abundance are found at all the investigated ages; this is consistent with predictions for rotationally induced mixing for low equatorial velocities (100–200 km s^{-1}). The observed $v \sin i$ velocities are considerably smaller than these limits, but we assume that most stars are rapidly rotating yet seen pole-on. Two stars appear to have depleted boron at a far faster rate than expected: HD 36591 and HD 205021 are very young stars in our program with no detectable boron. In Figure 14, they appear close to the locus for stars of 20 $M_\odot$ rotating at 450 km s^{-1}, but their locations in Figure 11 imply that the stars are very early main-sequence stars with masses of about 12–13 $M_\odot$. This discrepancy may indicate that rotationally induced mixing has been underestimated at high rotational

velocities or that it is more efficient then expected at lower masses.

The spectral window around the B III resonance lines proves well suited for a determination of the abundance of the iron group elements. For the local B-type stars in our sample, we show that they have an approximately solar metallicity. For the halo B-type star PG 0832+676, we find a low metallicity and an absence of boron which suggest that the star is probably a post-AGB star.

Further insights into rotationally induced mixing will require STIS spectra of additional rapidly rotating stars. A few stars examined by PQ01 have low boron upper limits and unenriched nitrogen and are ideal targets for follow-up studies. Additional stars that are sharp lined (low $v \sin i$), but rapidly rotating, are also suitable; however, in the absence of a way to extract the angle of inclination, information about abundances and rotation will require a statistical treatment. We also note that stars hotter than the present sample are not appropriate: the B III lines become too weak (see Fig. 7), and boron, present as the He-like ion, is lost to spectroscopic scrutiny.

Support for proposal GO 07400 was provided by NASA through a grant from the Space Telescope Science Institute, which is operated by the Association of Universities for Research in Astronomy, Inc., under NASA contract NAS 5-26555. K. A. V., M. L., and A. B. would also like to acknowledge research support from Macalester College and the Luce Foundation through a Clare Boothe Luce Professorship award. K. A. V. thanks Grace Mitchell and Claus Leitherer for help with the STIS data reductions and for STScI visitor funds. Many thanks to Charles Proffitt for helpful discussions, comments on the manuscript, and making his *IUE* data available for inspection. We also thank Katia Cunha for helpful discussions and Alex Heger for comments and for making recent model results available.

REFERENCES

Angulo, M., et al. 1999, Nucl. Phys. A, 656, 3
Blaauw, A. 1991, in The Physics of Star Formation and Early Stellar Evolution, NATO Advanced Science Institutes (ASI) Ser. C, Vol. 342, ed. C. J. Lada & N. D. Kylafis (Dordrecht: Kluwer), 125
Boesgaard, A. M., & Heacox, W. D. 1978, ApJ, 226, 888
Brown, A. G. A., de Geus, E. J., & de Zeeuw, P. T. 1994, A&A, 289, 101
Brown, A. G. A., & Verschueren, W. 1997, A&A, 319, 811
Brown, P. J. F., Dufton, P. L., Keenan, F., Boksenberg, A., King, D. L., & Pettini, M. 1989, ApJ, 339, 397
Cassinelli, J. P., Cohen, D. H., Macfarlane, J. J., Sanders, W. T., & Welsh, B. Y. 1994, ApJ, 421, 705
Crawford, D. L. 1963, ApJ, 137, 530
Cunha, K., & Lambert, D. L. 1994, ApJ, 426, 170 (CL94)
Cunha, K., Lambert, D. L., Lemke, M., Gies, D. R., & Roberts, L. C. 1997, ApJ, 478, 211
Cunha, K., Smith, V. V., Boesgaard, A., & Lambert, D. L. 2000a, ApJ, 530, 939
Cunha, K., Smith, V. V., & Lambert, D. L. 1998, ApJ, 493, 195
———. 1999, ApJ, 519, 844
Cunha, K., Smith, V. V., Parizot, E., & Lambert, D. L. 2000b, ApJ, 543, 850
de Jager, C. 1980, in GAM Vol. 19, The Brightest Stars (Dordrecht: Reidel), 50
de Zeeuw, P. T., Hoogerwerf, R., de Bruijne, J. H. J., Brown, A. G. A., & Blaauw, A. 1999, AJ, 117, 354
Ekberg, J. O. 1993, A&AS, 101, 1
Esteban, C., Peimbert, M., Torres-Peimbert, S., & Escalante, V. 1998, MNRAS, 295, 401
Fitch, W. S. 1969, ApJ, 158, 269
Fliegner, J., Langer, N., & Venn, K. A. 1996, A&A, 308, L13
Fukuda, I. 1982, PASP, 94, 271
Gies, D. R. 1987, ApJS, 64, 545
Gies, D. R., & Lambert, D. L. 1992, ApJ, 387, 673 (GL92)
Gold, M. 1984, Ph.D. thesis, Univ. München
Grebel, E. K., Richtler, T., & de Boer, K. S. 1992, A&A, 254, L5
Grevesse, N., & Sauval, A. J. 1998, Space Sci. Rev., 85, 161
Guthrie, B. N. G. 1984, MNRAS, 210, 159
Hadrava, P., & Harmanec, P. 1996, A&A, 315, L401
Hambly, N. C., Keenan, F. P., Dufton, P. L., Brown, P. J. F., Saffer, R. A., & Peterson, R. C. 1996, ApJ, 466, 1018
Heger, A., & Langer, N. 2000, ApJ, 544, 1016 (HL00)
Heger, A., Langer, N., & Woosley, S. E. 2000, ApJ, 528, 368
Herrero, A., Kudritzki, R. P., Vilchez, J. M., Kunze, D., Butler, K., & Haser, S. 1992, A&A, 261, 209
Heynderickx, D., Waelkens, C., & Smeyers, P. 1994, A&AS, 105, 447
Howk, J. C., Sembach, K. R., & Savage, B. D. 2000, ApJ, 543, 278
Ivans, I. I., et al. 1999, AJ, 118, 1273
Jerzykiewicz, M., & Pigulski, A. 1999, MNRAS, 310, 804
Jura, M., Meyer, D. M., Hawkins, I., & Cardelli, J. A. 1996, ApJ, 456, 598
Kilian, J. 1992, A&A, 262, 171
———. 1994, A&A, 282, 867
Korotin, S. A., Andrievsky, S. M., & Luck, R. E. 1999, A&A, 351, 168
Krzesiński, J., & Pigulski, A. 1997, A&A, 325, 987
Kurucz, R. L. 1979, ApJS, 40, 1
———. 1988, Trans. IAU, Vol. 20B, ed. M. McNally (Dordrecht: Kluwer)
Lambert, D. L. 2000, IAU Joint Discussion, Manchester
Lambert, D. L., Sheffer, Y., Federman, S. R., Cardelli, J. A., Sofia, U. J., & Knauth, D. C. 1998, ApJ, 494, 614
Langer, N., & Heger, A. 1999, in IAU Symp. 190, New Views of the Magellanic Clouds, ed. Y. H. Chu, N. Suntzeff, J. Hesser, & D. Bohlender (Dordrecht: Kluwer), 192
Lemke, M., Cunha, K., & Lambert, D. L. 2000, in The Galactic Halo: From Globular Cluster to Field Stars, Proc. of the 35th Liege International Astrophysics Colloq., ed. A. Noels, P. Magain, D. Caro, E. Jehin, G. Parmentier, & A. A. Thoul (Liege: Institut d'Astrophysique et de Geophysique), 223
Lennon, D. J., Brown, P. J. F., & Dufton, P. L. 1988, A&A, 195, 208
Maeder, A., & Meynet, G. 2000, A&A, 361, 159
Massey, P., Johnson, K. E., & Degioia-Eastwood, K. 1995, ApJ, 454, 151
Morton, D. C. 1991, ApJS, 77, 119
Olsen, E. H. 1977, Inf. Bull. Variable Stars, 1332, 1
Oosterhoff, P. T. 1937, Ann. Sternw. Leiden, 17, 1
Pigulski, A., & Jerzykiewicz, M. 1988, Acta Astron., 38, 401
Proffitt, C. R., Jönsson, P., Pickering, J. C., & Wahlgren, G. M. 1999, ApJ, 516, 342
Proffitt, C. R., & Quigley, M. F. 2001, ApJ, 548, 429 (PQ01)
Schoenberner, D., & Harmanec, P. 1995, A&A, 294, 509
Shima, M. 1963, Geochim. Cosmochim. Acta, 27, 991
Sneden, C., Kraft, R. P., Langer, G. E., Prosser, C. F., & Shetrone, M. D. 1992, AJ, 104, 2121
Tapia, M., Roth, M., & Navarro, S. 1984, in IAU Symp. 105, Observational Tests of the Stellar Evolution Theory, ed. A. Maeder & A. Renzini (Dordrecht: Kluwer), 353
Telting, J. H., Aerts, C., & Mathias, P. 1997, A&A, 322, 493
Thielemann, F., et al. 1995, Stellar Reaction Rates
Venn, K. A., Lambert, D. L., & Lemke, M. 1996, A&A, 307, 849
Vrancken, M., Lennon, D. J., Dufton, P. L., & Lambert, D. L. 2000, A&A, 358, 639
Warren, W. H., Jr., & Hesser, J. E. 1978, ApJS, 36, 497
Wellstein, S. 2000, Ph.D. thesis, Univ. Potsdam
Wellstein, S., Langer, N., & Braun, H. 2001, A&A, 369, 939
Zhai, M., & Shaw, D. M. 1994, Meteoritics, 29, 607